NUMERICAL MODEL FOR CALCULATION OF HYDRAULIC TRANSIENT WITH COLUMN SEPARATION AND FLUID-STRUCTURE INTERACTION

M.S. Rocha[1], J. Campos[1], P.Rocha[1]; M. Camargo[1]

[1] Instituto de Pesquisas Energéticas e Nucleares – IPEN/CNEN-SP

marcelo.rocha@usp.br, jaac2108@usp.br,

pedrohenriquenrocha@gmail.com, micelli.camargo@gmail.com

ABSTRACT

This paper presents a study of the phenomenon and the development of a computational code for water hammer with column separation and fluid-structure interaction (FSI) in one-dimensional. FSI model was considered as an initial and boundary value problem, represented by a system of hyperbolic partial differential equations that simultaneously describes the propagation of pressure waves in the liquid and axial stress waves in the structure. Column separation is treated as a boundary condition. Method of characteristics, combined with linear interpolations, was used to solve the system of hyperbolic partial differential equations. The proposed numerical model was compared to experimental data from the base article (BERGANT, ANTON et al., 2005) provided by author, for a system consisting of a reservoir with a constant upstream level, a single straight pipe and a downstream valve with rigid fixation.

Keywords: Hydraulic transients,water hammer, fluid structure interaction, cavitation, column separation.

1 SYMBOLISM AND ABBREVIATIONS

1D - One dimension

2D - Two dimensions

c - Speed of sound in the fluid, [m/s]

c_0 - Speed of sound in the unconfined fluid, [m/s]

c_1 - Speed of sound in the incompressible fluid in an elastic tube, [m/s]

$\tilde{c}_f$ - Adjusted speed of sound in the fluid, [m/s]

c_f - Actual speed of sound in the fluid, [m/s]

c_t - Wave speed in the tube wall, [m/s]

$\tilde{c}_t$ - Adjusted wave speed in the tube wall, [m/s]

C^- - Negative characteristic equation

C^+ - Positive characteristic equation

CFL - Courant-Friedrich-Lewy

Din - Internal diameter of the pipe, [m²]

DVCM - Discrete Vapor Cavity Model

dx - Infinitesimal spacing (grid) of the mesh in space, [m]

dy - Infinitesimal spacing (grid) of the mesh in time, [s]

E - Young's modulus, [Pa]

e - Wall thickness of the pipe, [m]

ODE - Ordinary differential equation

PDE - Partial differential equation

f - Darcy-Weisbach friction factor

H - Piezometric head

H_b - Barometric head, [m]

H_0 - Piezometric head in steady-state, [m]

H_i^t - Piezometric head at point i and time t, [m]

$H_{i+1}^{t-\Delta t}$ - Piezometric head at point (i+1) and time (t-Δt), [m]

$H_{i-1}^{t-\Delta t}$ - Piezometric head at point (i-1) and time (t-Δt), [m]

H_{max} - Maximum head, [m]

H_{mp} - Head at the longitudinal midpoint of the pipeline, [m]

H_{res} - Head at the reservoir, [m]

H_{vap} - Vapor head at temperature T, [m]

i - Spatial step

FSI – Fluid structure interaction

j - Time step

Kf - Fluid bulk modulus

l - Maximum length of the vapor cavity

m - Adjustable constant

MOC - Method of characteristics

CN - Courant number

P or p - Pressure, [Pa]

$\bar{P}$ - Average axial pressure, [Pa]

P_{ext} - External pressure, [Pa]

P_{vap} - Absolute vapor pressure at temperature T, [Pa]

$(Q_{in})_i^t$ - Inlet flow rate at point i and time t, [m³/s]

Q_i^t - Flow rate at point i and time t, [m³/s]

$(Q_{in})_{i+1}^{t-\Delta t}$ - Inlet flow rate at point (i+1) and time (t-Δt), [m³/s]

$Q_{i-1}^{t-\Delta t}$ - Flow rate at point (i-1) and time (t-Δt), [m³/s]

Q_0- Flow rate in steady-state, [m³/s]

Q_v- Discharge flow rate at the valve, [m³/s]

r - Radial coordinate

R_{in} - Internal radius of the pipe, [m²]

T - Temperature, [ºC]

t - Time, [s]

tc - Actual valve closure time, [s]

HT - Hydraulic transient

u_x- Longitudinal displacement of the pipe, [m]

$\dot{u}_x$- Axial velocity of the pipe, [m/s]

$\overline{\dot{u}_x}$ - Average axial velocity of the pipe, [m/s]

$\ddot{u}_x$- Longitudinal acceleration of the pipe, [m/s²]

$\dot{u}_r$ - Radial velocity of the pipe, [m/s]

$\overline{\dot{u}_r}$ - Average radial velocity of the pipe, [m/s]

V - Volume, [m³]

CV - Control volume

V_{cv}- - Vapor cavity volume, [m³]

v_f- Fluid velocity, [m/s]

v_r- Radial fluid velocity, [m/s]

$v_{r,ext}$ - External radial fluid velocity, [m/s]

$v_{rel,f}$- Relative velocity between the fluid and the pipe wall, [m/s]

v_x- Axial fluid velocity, [m/s]

v_0- Fluid velocity, [m/s]

$\bar{v}$- Average axial velocity, [m/s]

x - Spatial longitudinal coordinate

α - Vapor fraction

ΔH - Instantaneous increase in head predicted by Joukowsky, [m]

ΔH_v- Head decrease at the valve, [m]

∆P - Pressure variation, [Pa]

∆v - Velocity variation, [m/s]

Δv_{cv}- Decrease in the fluid return velocity, [m/s]

∆x - Spacing (grid) of the mesh in space, [m]

∆y - Spacing (grid) of the mesh in time, [s]

μ_f- Dynamic viscosity of the fluid, [Pa.s]

υ - Poisson's ratio, [Pa]

θ - Inclination of the pipe relative to the reference level, [rad]

ρ_f – Fluid specific mass, [kg/m³]

ρ_t - Pipe material specific mass, [kg/m³]

ψ - Numerical weighting factor

γ_f - Fluid specific weight, [N/m³]

τ_v- Dimensionless valve closure time constant

τ_{xr} or τ_{rx}- Shear stress, [N/m²]

σ_{mp} - axial stress at midpoint of pipe, [N/m²]

σ_r- Radial stress, [N/m²]

σ_x- Axial stress, [N/m²]

$\overline{\sigma_x}$ - Average axial stress, [N/m²]

σ_ϕ - Circumferential stress, [N/m²]

$\overline{\sigma_\phi}$ - Average circumferential stress, [N/m²]

2 INTRODUCTION

Mainly, fluid transportation research and engineering projects primarily focus on steady-state flow. However, sudden changes in flow conditions caused by rapid valve operations, pump startups, or shutdowns give rise to hydraulic transients. These transients induce significant dynamic forces within pipeline systems due to sudden pressure fluctuations, impacting the propagation of pressure waves. Such forces lead to fluid-structure interaction (FSI), where the pipeline system and the fluid cannot be treated separately during theoretical analysis, necessitating the consideration of interaction mechanisms. Thus, accurately modeling this physical phenomenon becomes crucial for proper pipeline sizing, selection of valve closing times, and prevention of damage. This article introduces the implementation of a *Python*® numerical model for a liquid-filled pipeline, with and without column separation, while incorporating the combined effects of fluid-structure interaction within a reservoir-pipeline-valve system. The model employs one-dimensional (1D) governing equations derived from integrating the general three-dimensional (3D) equations for both the fluid and structure. The fluid-structure interaction mechanism encompasses Poisson and friction couplings. The Darcy-Weisbach friction model is employed for the fluid, and the boundary conditions incorporate the Discrete Vapor Cavity Model (DVCM) to account for column separation effects. The essential equations specific to the pipeline under consideration are formulated as a set of four hyperbolic partial differential equations (PDEs) and solved using the method of characteristics (MOC).

3 THEORY AND NUMERICAL MODEL

A one-dimensional mathematical model describing transient behavior in a fully liquid-filled pipeline will be presented. This model is based on classical hydraulic transient theory and beam theory, considering Fluid Structure Interaction (FSI) and column separation effects.

The symbols used in the equations are defined in the "Symbols and Abbreviations" section.

To facilitate comprehension, the modeling will be discussed separately for the fluid, pipe, and fluid-structure aspects, considering the following conditions.

Pipe:

- Straight, slender, thin-walled, and circular cross-section;
- Homogeneous, isotropic material and linearly;
- Immersed in a non-viscous fluid;
- No restrictions on its axial movement;
- Subject to small deformations;
- Instantaneous closure valve with restrictions on its axial movement; and
- Radial motion resistance due to inertia, shear deformation, and bending stiffness are neglected.

Fluid:

- Newtonian and homogeneous;
- Isotropic and linearly elastic; and
- Free or dissolved gas in the liquid is considered small.

The fluid-pipe system is subject to isothermal conditions, quasi-stationary fluid-structure friction, and modeled in one dimension with an axial coordinate along the centerline of the pipe. This approximation is valid for long wavelengths or low frequencies (TIJSSELING, 1993).

Fluid and pipe velocities are considered much smaller than the wave velocity ($c_f \gg v$ and $c_t \gg \dot{u}_x$), therefore convective terms are neglected.

The cavitation model employed in this study is based on the vaporization phenomenon. It assumes that whenever there are bubbles present, the pressure within the fluid equals the vapor pressure of the fluid.

3.1 Hydraulic Transients (HT)

When the conditions of a steady flow are altered over time, we have a transient flow, which is referred to as Hydraulic Transients (TH). TH is an unstable flow in a pipeline system filled with liquid fluid, generated by sudden changes in the fluid flow conditions. These changes are usually related to rapid valve closure and opening, pump start-up and shutdown, pipe rupture (TIJSSELING, 1993). During these events, hydraulic systems experience specific loads or forces due to variations in fluid momentum.

The current theory of TH is based on the research of Joukowsky (1898) and Allievi (1903), which were studies conducted on a pipeline where water flows from a reservoir and is suddenly interrupted, causing a hydraulic transient (U.S. NUCLEAR REGULATORY RESEARCH, 1997). The resulting pressure wave from this transient travels back to the source reservoir at the speed of sound. This increase in pressure is given by equation (1).

$$\Delta P = \rho_f c_f \Delta v \tag{1}$$

Equation (1) relates the pressure change ∆P to the velocity change ∆v through the constant value $\rho_f c_f$.

Joukowsky used the speed of sound, which takes into account the compressibility of the fluid and the elasticity of the tube walls. Until the 1960s, the graphical method was used for the mathematical treatment of hydraulic transients. However, with the advent of computers, the Method of Characteristics (MOC) became the standard for an approximate numerical solution of these transients (TIJSSELING, 1993).

Equations of HT are applied when the pressure is above the vapor pressure. They consist of the continuity equation and the momentum equation.

Continuity equation (mass conservation) neglecting convective terms:

$$\frac{\partial \mathrm{H}}{\partial \mathrm{t}} + \frac{c^2}{gA_{in}} \frac{\partial Q}{\partial \mathrm{x}} + \frac{Qsen(\theta)}{A_{in}} = 0 \tag{2}$$

Momentum equation, neglecting convective terms:

$$\frac{\partial \mathrm{H}}{\partial \mathrm{x}} + \frac{1}{gA_{in}} \frac{\partial Q}{\partial \mathrm{t}} + \frac{fQ|Q|}{2g{A_{in}}^2 D_{in}} = 0 \tag{3}$$

3.2 Cavitation and Column Separation

Low pressures during transient events in pipelines often result in cavitation. The term cavitation is used to describe the formation and growth of cavities in the liquid due to a transient in which the local pressure has been reduced to the vapor pressure of the liquid.

Location and intensity of cavitation are influenced by various system parameters, including the type of transient (rapid valve closure, pump failure, turbine load rejection), system layout (pipe dimensions, valve profile and positioning), and fluid transport process characteristics (fluid flow rate, system head, pipe wall friction, and fluid properties) (BERGANT, ANTON; SIMPSON, 1999).

Depending on the pipe geometry and fluid velocity gradient, these cavities can grow and coalesce to the point of filling the pipe's cross-section, leading to column separation (CHAUDHRY, 2014).

In regions of low pressure, rarefaction waves are reflected as positive waves (e.g., from a reservoir), compressing the bubbles in the cavitating flow region and progressively reducing the size of the cavity produced by column separation. Consequently, the cavity collapses, and the separated columns join, resulting in very high pressures (CHAUDHRY, 2014).

Cavitation significantly alters the shape of the pressure wave, and the classical equations of TH for liquid flow are no longer valid (BERGANT, ANTON et al., 2008) since the single-phase flow becomes two-phase.

Joukowsky (1898) described mathematically many of the physical aspects of the pressure wave and its propagation in liquid systems and was the first to observe and understand the phenomenon of column separation. A section of his work is literally transcribed in (BERGANT, A. et al., 2004). In (BERGANT, ANTON et al., 2006), a synthesis of TH with cavitation is provided, describing the development of pressure spikes after the collapse of a vapor cavity.

(FAN; TIJSSELING, 1992) based their measurements on the structural time scale of vibration in a closed pipe excited by external impact. (BERGANT, ANTON; SIMPSON, 1999) conducted a parametric numerical analysis in a reservoir-pipe-valve system to calculate critical flow conditions that exhibit different types of column separation according to the maximum head. They classified transient regimes based on the physical state of the fluid and the maximum pressure in the pipeline. Meanwhile, (FANELLI, 2000) summarized the experimental work

conducted between 1971-1991 by (IAHR, 2000) to develop and validate models implemented in computer codes. (BERNARD, 2013) qualitatively classified transient regimes as follows (BERGANT, ANTON et al., 2006):

- No cavitation;
- Cavitation, but the cavity does not collapse;
- Cavitation with cavity collapse but without high pressures; and
- Cavitation with cavity collapse and excessive pressures.

3.2.1 Discrete Vapor Cavity Model (DVCM)

The discrete vapor cavity model is the most widely used model for column separation and cavitation. Its significant advantage is being an easily implemented model that reproduces many characteristics of the physical events of column separation in pipelines (BERGANT, A. et al., 2004).

Figure 1 - Representation of the discrete cavity model.

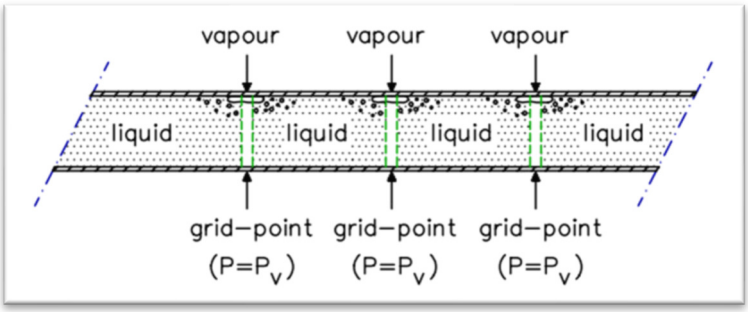

Source: (TIJSSELING, 1996).

The DVCM methodology is detailed in (WYLIE, E. B.; STREETER, 1978).

Vapor cavities can form in any of the computational sections if the calculated pressure falls below the vapor pressure of the liquid. This method does not differentiate between localized vapor cavities and distributed vapor cavitation (SIMPSON, A.; WYLIE, E., 1989).

The method is, therefore, a simplistic approximation of the real physical situation since a constant wave velocity of c is assumed for both the two-phase (HT) and column separation regions. Thus, the DVCM converts the actual partial differential equations with a non-constant wave velocity (for regions with vapor cavities) into different partial differential equations (with assumed constant wave velocity) and then attempts to correct the error(s) in the discrete vapor cavity limit(s) (SIMPSON; BERGANT, 1994b).

For this modeling, vapor cavities are confined to computational sections (meshes), and a constant wave velocity of pressure is assumed for the fluid between mesh points, as shown in Figure 1. When a vapor cavity forms, this computational section is treated as a fixed internal boundary condition. The pressure in this section is set to the vapor pressure of the liquid until the cavity collapses.

Both the inlets and outlets of the computational sections are calculated using compatibility equations for each of the positive and negative characteristic equations (C+ and C-) within the method of characteristics (MOC).

Figure 2 - Method of characteristics - stepped mesh for reservoir-pipeline-valve system.

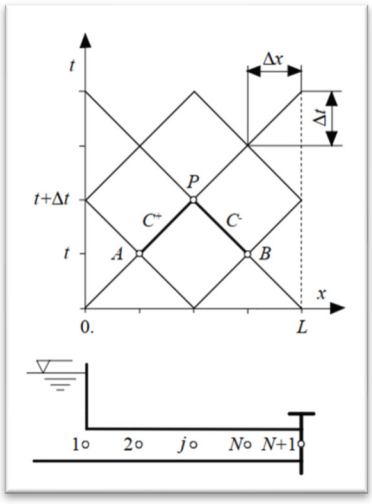

Source: (BERGANT, ANTON et al., 2006).

Compatibility equations for the configuration illustrated in Figure 2 are as follows, with index i representing the spatial step (x-axis):

$$C^+: H_i^t = CP - BQ_i^t \tag{4}$$

$$C^-: H_i^t = CM + BQ_i^t \tag{5}$$

$$CP = H_{i-1}^{t-\Delta t} + BQ_{i-1}^{t-\Delta t} - RQ_{i-1}^{t-\Delta t}\left|Q_{i-1}^{t-\Delta t}\right| \tag{6}$$

$$CM = H_{i+1}^{t-\Delta t} - BQ_{i+1}^{t-\Delta t} + RQ_{i+1}^{t-\Delta t}\left|Q_{i+1}^{t-\Delta t}\right| \tag{7}$$

$$B = \frac{c}{gA_{in}} \tag{8}$$

$$R = \frac{f.\Delta x}{2gA_{in}{}^{2}D_{in}} \tag{9}$$

From (4) e (5), H_i^t can be obtained:

$$H_i^t = \frac{CP + CM}{2} \tag{10}$$

The flow rate at point i and time t is obtained by:

$$Q_i^t = \frac{H_i^t - CM}{B} \tag{11}$$

In the DVCM, the inlet ($Q_{in,}$) and outlet (Q) flow rates at point P can be different. In finite differences, equations (4) and (5) at index P i (spatial step) become (BERGANT, A. et al., 2006):

$$H_i^t - H_{i-1}^{t-\Delta t} + \frac{c}{gA_{in}}\left[(Q_{in})_i^t - Q_{i-1}^{t-\Delta t}\right] + \frac{f\Delta x(Q_{in})_i^t\left|Q_{i-1}^{t-\Delta t}\right|}{2gA_{in}{}^{2}D_{in}} = 0 \tag{12}$$

$$H_i^t - H_{i+1}^{t-\Delta t} + \frac{c}{gA_{in}}\left[Q_i^t - (Q_{in})_{i+1}^{t-\Delta t}\right] - \frac{f\Delta xQ_i^t\left|(Q_{in})_{i+1}^{t-\Delta t}\right|}{2gA_{in}{}^{2}D_{in}} = 0 \tag{13}$$

$$CP_{bifásico} = H_{i-1}^{t-\Delta t} + BQ_{i-1}^{t-\Delta t} - RQ_{i-1}^{t-\Delta t}\left|Q_{i-1}^{t-\Delta t}\right| \tag{14}$$

It can be observed from Figure 3 that there is a modification in the volumetric flow rates in the computational section where column separation occurs, which influences the formulation of the negative characteristic equation (C^-), as it has its initial point at $(Q_{in})_{i+1}^{t-\Delta t}$ rather than $Q_{i+1}^{t-\Delta t}$. Thus, $Q_{i+1}^{t-\Delta t}$ has been replaced by $(Q_{in})_{i+1}^{t-\Delta t}$ in equation (7), resulting in:

$$CM_{bifásico} = H_{i+1}^{t-\Delta t} - B(Q_{in})_{i+1}^{t-\Delta t} + R(Q_{in})_{i+1}^{t-\Delta t}\left|(Q_{in})_{i+1}^{t-\Delta t}\right| \tag{15}$$

Head in the computational section where column separation occurs is given by:

$$H_i^t = \frac{CP_{bifásico} + CM_{bifásico}}{2} \tag{16}$$

When the pressure becomes lower or equal to the vapor pressure, the nodes are treated as boundary nodes with a fixed pressure as described in equation (17):

$$H_{vap} = H_0 - \frac{P_{ext}}{\rho_f g} + \frac{P_{vap}}{\rho_f g} \tag{17}$$

The inlet flow rate at point i and time t is calculated by:

$$(Q_{in})_i^t = \frac{CP_{bifásico} - H_i^t}{B} \tag{18}$$

Vapor cavity volume (V_{cv}) in a computational section in terms of the downstream and upstream flow rate difference at point P is:

$$V_{cv} = \int_t^{t+\Delta t} [Q_i - (Q_{in})_i] dt \tag{19}$$

Figure 3 - Grid for the MOC with two-phase fluid..

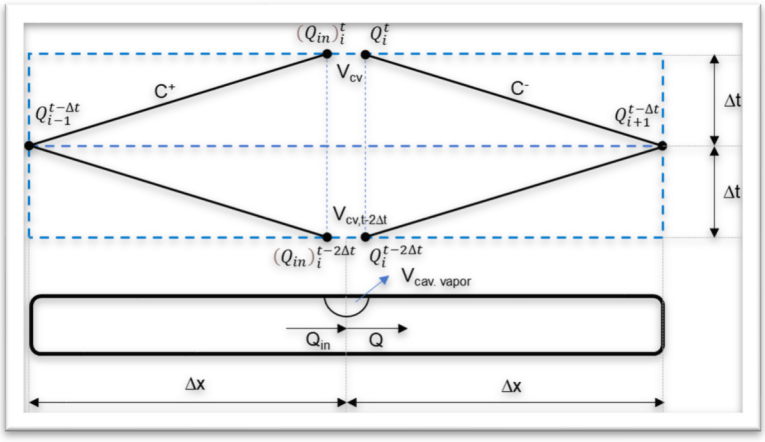

Adapted from (JENSEN et al., 2018).

The numerical integration of equation (19) in MOC with the discretization used in Figure 3 is given by:

$$Vcv^{t} = Vcv^{t-2\Delta t} + \Psi(Q_i^t - (Q_{in})_i^t) + 2\Delta t(1-\psi)\left(Q_i^{t-2\Delta t} - (Q_{in})_i^{t-2\Delta t}\right) \quad (20)$$

In which Vcv^{t} and $Vcv^{t-2\Delta t}$ are the volumes of vapor cavities at the current time and *2Δt* ago, and ψ is a numerical weighting factor.

When volume of the vapor cavity becomes zero, it means that the collapse of this cavity has occurred. Then, the system can be treated as single-phase, and calculation of the HT (two-phase flow) returns to the standard procedure, where $(Q_{in})_i^t = Q_i^t$.

The compatibility equations ((4), (5), (12), and (13)) are valid along the length of the pipeline (0 < x < L), and boundary conditions are required (*x = 0 e x = L*).

3.3 Fluid Structure Interaction (FSI):

In the past, researchers made it clear that classical two-phase flow theory (WYLIE, E.B.; STREETER, 1978) was sufficient and adequate to predict extreme loads in a system as long as it is rigidly anchored. However, when a pipeline system has certain degrees of freedom, significant deviations from classical theory can occur due to system movement.

FSI is essentially a dynamic phenomenon in which the interaction is always caused by dynamic forces acting simultaneously on the fluid and pipeline. This interaction involves the transfer of momentum and forces between pipeline and fluid during transient flow, manifesting as pipe vibration and disturbances in the velocity and pressure of fluid (WIGGERT; TIJSSELING, 2001).

There are three mechanisms that couple the dynamic behavior of the fluid and the pipeline system (TIJSSELING; LAVOOIJ, 1990):

- Friction coupling: represents the mutual friction between the fluid and the pipe;
- Poisson coupling: relates fluid pressures to axial stresses in the pipe through the contraction or expansion of its wall. Poisson coupling leads to precursor waves induced by disturbances in the fluid that travel faster than the wave front of classical two-phase flow; and

- Connection coupling: describes the local forces acting mutually between the fluid and the pipeline system.

Friction and Poisson coupling act throughout the pipeline system, while connection coupling occurs only at specific locations, such as in line accessories (valves, fittings, elbows).

3.3.1 Fluid bulk modulus (K_f)

The fluid bulk modulus is the property that relates pressure changes to volume changes (e.g., expansion and compression) (CROWE et al., 2009). The volume change is related to the change in fluid specific mass.

For a fluid with a specific mass (ρ_f) subjected to a pressure increment dP necessary to induce a variation ($d\rho_f / \rho_f$):

$$K_f = \frac{dP}{d\rho_f \Big/ \rho_f} \tag{21}$$

3.3.2 Sound velocity in fluid (c)

Compressibility term of the fluid will be expressed through the equation of state that relates fluid specific mass to the pressure.

State equation:

$$\frac{\partial \rho_f}{\partial P} = \frac{\rho_f}{K_f} \tag{22}$$

Variables ρ_f and K are functions of (P, T).

For confined fluids in tubes, the speed of sound is significantly lower. HELMHOLTZ (1848) was the first to suggest that the decrease in velocity is due to the effect of tube elasticity, but theoretical model for this phenomenon in compressible fluids in elastic tubes emerged decades later with (KORTEWEG, 1878).

Speed of sound in an unconfined fluid (c_0) is given by:

$$c_0 = \sqrt{\frac{K_f}{\rho_f}} \tag{23}$$

Speed of sound in a confined compressible fluid (c_f) in a flexible tube is given by (KORTEWEG, 1878):

$$\frac{1}{{c_f}^2} = \frac{1}{{c_0}^2} + \frac{1}{{c_1}^2} \tag{24}$$

$$c_1 = \sqrt{\frac{Ee}{\rho_f D_{in}}} \tag{25}$$

Studies conducted by (HALLIWELL, 1963), discrepancy in theoretical wave velocity formulas was discussed, and this difference was attributed to how the pipe supports are considered. In order to reduce the difference, a correction factor (ψ) was introduced, which is a function of the Poisson's ratio, in the wave equation model to account for different supports (WYLIE, E. B.; STREETER, 1978).

- ψ = 1: for a pipe anchored with expansion joints along its entire length, the axial stress is negligible;
- ψ = 1 - υ^2: for a fully anchored pipe that restricts axial movement, the axial displacements are negligible;
- ψ = 1 − υ /2: for a pipe anchored only upstream, the axial stress on the pipe wall is considered proportional to the fluid pressure acting on an unrestricted closed valve downstream.

Thus, equation (24) is rewritten as:

$$c_f = \sqrt{\frac{K_f}{\rho_f}\left(1 + \psi\frac{D_{in}K_f}{eE}\right)^{-1}} \tag{26}$$

Equation (26) provides the velocity of the pressure wave (c_f) used for classical HT calculations (TIJSSELING, 1996).

3.3.3 Governing Equations:

Fluid and the pipe interact through coupled radial motion. The development of these equations, in 1D, can be found in (TIJSSELING, 1993).

Fluid:

Starting point is the continuity and Navier-Stokes equations in 2D, expressed in cylindrical coordinates, where x represents the axial axis and r represents the radial axis. Assuming an isothermal condition, $p << K_f$, convective terms ($c_0 >> v_x$ e v_r) are neglected, and radial forces due to gravitational effects are disregarded due to axial symmetry. Thus, we have:

Continuity equation:

$$\frac{1}{K_f}\frac{\partial \bar{P}}{\partial t} + \frac{\partial \bar{v}}{\partial x} + \frac{2}{R_{in}} v_r|_{r=R_{in}} = 0 \tag{27}$$

Axial momentum equation:

$$\rho_f \frac{\partial \bar{v}}{\partial t} + \frac{\partial \bar{P}}{\partial x} = \rho_f g sen\theta - \frac{2}{R_{in}}\tau_0 \tag{28}$$

For Newtonian fluid:

$$\tau_0 = -\mu_f \left.\frac{\partial v_x}{\partial r}\right|_{r=R_{in}} \tag{29}$$

Radial momentum equation:

$$\frac{1}{2}\rho_f R_{in} \left.\frac{\partial v_r}{\partial t}\right|_{r=R_{in}} + p|_{r=R_{in}} - \bar{P} = 0 \tag{30}$$

Pipe:

Starting point is two momentum equations expressed in cylindrical coordinates, where *x* represents the axial axis and *r* represents the radial axis. The effects of bending resistance, rotational inertia, transverse shear, convective terms, and gravitational forces acting on the pipe are neglected. The specific mass of the pipe material (ρ_t) is assumed to be constant. The simplified 1D equations are as follows:

Axial momentum equation:

$$\rho_t \frac{\partial \overline{\dot{u}_x}}{\partial t} = \frac{\partial \overline{\sigma_x}}{\partial x} + \frac{(R_{in}+e)}{(R_{in}+0{,}5e)e}\tau_{xr}|_{r=(R_{in}+e)} - \frac{R_{in}}{(R_{in}+0{,}5e)e}\tau_{xr}|_{r=R_{in}} + \rho_t g sen\theta \tag{31}$$

Radial momentum equation:

$$\rho_t \frac{\partial \overline{\dot{u}_r}}{\partial t} = \frac{(R_{in}+e)}{(R_{in}+0{,}5e)e}\sigma_r|_{r=(R_{in}+e)} - \frac{R_{in}}{(R_{in}+0{,}5e)e}\sigma_r|_{r=R_{in}} - \frac{1}{(R_{in}+0{,}5e)}\overline{\sigma_\phi} \tag{32}$$

Where:

$$\overline{\dot{u}_x} = \frac{1}{2\pi(R_{in}+0{,}5e)e}\int_{R_{in}}^{(R_{in}+e)} 2\pi r\, \dot{u}_x\, dr \tag{33}$$

$$\overline{\dot{u}_r} = \frac{1}{2\pi(R_{in}+0{,}5e)e}\int_{R_{in}}^{(R_{in}+e)} 2\pi r\, \dot{u}_r\, dr \tag{34}$$

$$\overline{\sigma_x} = \frac{1}{2\pi(R_{in}+0{,}5e)e}\int_{R_{in}}^{(R_{in}+e)} 2\pi r\, \sigma_x\, dr \tag{35}$$

$$\overline{\sigma_\phi} = \frac{1}{e}\int_{R_{in}}^{(R_{in}+e)} \sigma_\phi\, dr \tag{36}$$

Stress-strain relationships complete mathematical model and are provided by the generalized Hooke's law:

$$\frac{\partial\overline{\sigma_x}}{\partial t} = E\frac{\partial\overline{\dot{u}_x}}{\partial x} + \upsilon\frac{\partial\overline{\overline{\sigma_\phi}}}{\partial t} + \upsilon\frac{\partial\overline{\sigma_r}}{\partial t} \tag{37}$$

$$\overline{\overline{\sigma_\phi}} = \frac{1}{2\pi(R_{in}+0{,}5e)e}\int_{R_{in}}^{(R_{in}+e)} 2\pi\, \sigma_\phi\, dr \tag{38}$$

$$\overline{\sigma_r} = \frac{1}{2\pi(R_{in}+0{,}5e)e}\int_{R_{in}}^{(R_{in}+e)} 2\pi\, \sigma_r\, dr \tag{39}$$

Fluid structure coupling:

Fluid and pipe equations are coupled through boundary conditions that represent the contact between the fluid and the pipe wall at the interface $r = R_{in}$. It is assumed that there is a constant pressure (P_{ext}) outer of the pipe.

Boundary conditions at the interface are:

$$\tau_{xr}|_{r=R_{in}} = -\tau_0 \qquad \tau_{xr}|_{r=(R_{in}+e)} = 0 \tag{40}$$

$$\sigma_r|_{r=R_{in}} = -p|_{r=R_{in}} \qquad \sigma_r|_{r=(R_{in}+e)} = -P_{ext} \tag{41}$$

$$\dot{u}_r|_{r=R_{in}} = -v_r|_{r=R_{in}} \qquad \dot{u}_r|_{r=(R_{in}+e)} = v_{r,ext} \tag{42}$$

Using Darcy-Weisbach friction factor (f), 1D model of four equations, with unknowns H, v, σ_x and $\dot{u}_x$ (LAVOOIJ; TIJSSELING, 1991), is presented below.

<u>Fluid:</u>

Continuity equation:

$$\frac{\partial v_f}{\partial t} + g\frac{\partial H}{\partial x} = -\frac{f}{4R_{in}} v_{rel,f}\left|v_{rel,f}\right| \tag{43}$$

Axial momentum equation:

$$\frac{\partial v_f}{\partial x} + \frac{g}{c_f^2}\frac{\partial H}{\partial t} = 2\upsilon\frac{\partial \dot{u}_x}{\partial x} \tag{44}$$

Pipe:

Axial momentum equation:

$$\frac{\partial \dot{u}_x}{\partial t} - \frac{1}{\rho_t}\frac{\partial \sigma_x}{\partial x} = \frac{\rho_f}{\rho_t}\frac{A_{in}}{A_t}\frac{f}{4R_{in}} v_{rel,f}\left|v_{rel,f}\right| + gsen\theta \tag{45}$$

$$\frac{\partial \dot{u}_x}{\partial x} - \frac{1}{\rho_t c_t^2}\frac{\partial \sigma_x}{\partial t} = -\rho_f g\frac{R_{in}\,\upsilon}{eE}\frac{\partial H}{\partial t} \tag{46}$$

$$v_{rel,f} = v_f - \dot{u}_x \tag{47}$$

$$c_t^2 = \frac{E}{\rho_t} \tag{48}$$

3.4 Boundary conditions

3.4.1 Reservoir

It is assumed that the reservoir is large enough so that the fluid level elevation during operation can be neglected, and head in the reservoir (H_{res}) is considered constant.

$$H = H_{res} \tag{49}$$

$$u_x = 0 \tag{50}$$

3.4.2 Steady-State – initial condition

Initial condition is the solution of basic equations for steady-state (TIJSSELING, 1993).

$$H(x,0) = H_{res} - \rho_f \left(\frac{f}{4R_{in}} v_{rel,f} \left| v_{rel,f} \right| - g sen\theta \right) x \tag{51}$$

$$v_f(x,0) = constante \tag{52}$$

$$\bar{\sigma}_x(x,0) = \bar{\sigma}_x(0,0) - \left[\frac{1}{\left(e + \frac{e^2}{2R_{in}} \right)} \frac{\rho_f f}{8} v_{rel,f} \left| v_{rel,f} \right| + \rho_t \, g \, sen\theta \right] x \tag{53}$$

$$\overline{\dot{u}_x}(x,0) = 0 \tag{54}$$

3.4.3 Valve

Each valve has different cavitation characteristics, flow rates, and torques. Cavitation is a complex subject, and accurate modeling of valve closure is important as it affects the magnitude and shape of the resulting pressure peak (JENSEN et al., 2018).

The behavior of the valve can be approximated by (WYLIE, E.B.; STREETER, 1978):

$$\tau_v = 1 - \left(\frac{t}{t_c} \right)^m \tag{55}$$

Constant m is adjustable. If m is set to zero for an instantaneous closure valve, it produces the maximum pressure peak.

The valve discharge flow rate (Q_v) for any opening is given by:

$$Q_v = \frac{Q_0}{\sqrt{H_0}} \tau_v \sqrt{\Delta H} \tag{56}$$

In this case, ΔH represents the pressure drop across the valve. By simultaneously solving equations (4) and (56):

$$Q_P = -BC_v + \sqrt{(BC_v)^2 + 2C_v CP} \tag{57}$$

$$C_v = \frac{(Q_0 \tau_v)^2}{2H_0} \tag{58}$$

Conditions for an instantaneous closure fixed valve (LAVOOIJ; TIJSSELING, 1991):

$$v_f(L,t) = 0 \tag{59}$$

$$u_x = 0 \tag{60}$$

3.4.4 Column separation

In the computational section where column separation occurs, it is not allowed for local absolute pressure (P_{abs}) to be lower than the vapor pressure (P_{vap}) of fluid. In this section, the following condition is imposed:

$$P_{abs} = P_{vap} \tag{61}$$

Which is equivalent to:

$$H_{vap} = H_0 - x\ sen\theta - \frac{P_{ext}}{\rho_f g} + \frac{P_{vap}}{\rho_f g} \tag{62}$$

Volume of vapor cavity is calculated as:

$$V_{cv} = V_{cv}(t - 2\Delta t) \pm A_{in}\left[v_f(t) - \dot{u}_x(t)\right]\Delta t \tag{63}$$

Vapor cavity collapses when $V_{cv} = 0$.

When absolute pressure equals vapor pressure, vapor cavities appear. In the present model, cavities are concentrated in the computational section (*i*). Between the sections, it is assumed that pure liquid exists, where the basic HT equations (43) to (46) remain valid. This means that the velocity of the pressure wave $\tilde{c}_f$ is maintained between the points i. However, pressure waves do not propagate through the cavitation region since constant vapor pressure is assumed. The collapse of the vapor cavity caused by the pressure wave results in a delay in propagation, which is observed as a reduction in wave velocity (TIJSSELING, 1993).

3.5 Method of characteristics (MOC)

A significant portion of HT analysis is carried out using codes based on MOC due to the simplicity of treating a constant time increment and adopting a staggered discretization (SHARP; SHARP, 1996). MOC is a mathematical procedure for obtaining a general wave propagation solution. The solution describes characteristic lines (C^- and C^+) in an x-t plane of wave propagation, where the functions of *v* and *H* are constant. When characteristic lines intersect, local values for *v* and *H* are determined (MOODY, 1990).

By applying the MOC to governing equations, (43) to (46) (TIJSSELING, 1993):

Fluid:

$$\frac{dv_f}{d_t}+\frac{g}{c_f}\left\{\left(\frac{\tilde{c}_f}{c_f}\right)+2\upsilon^2\,\frac{R_{in}}{e}\frac{\rho_f}{\rho_t}\frac{(c_f\tilde{c}_f)/c_t^2}{\left[1-\left(\tilde{c}_f/c_t\right)^2\right]}\right\}\frac{dH}{dt}+2\upsilon\frac{\left(\tilde{c}_f/c_t\right)^2}{\left[1-\left(\tilde{c}_f/c_t\right)^2\right]}\left(\frac{d\dot{u}_x}{dt}\right)$$
$$-\frac{2\upsilon}{\rho_t\tilde{c}_f}\frac{\left(\tilde{c}_f/c_t\right)^2}{\left[1-\left(\tilde{c}_f/c_t\right)^2\right]}\left(\frac{d\sigma_x}{dt}\right) \tag{64}$$
$$=-\frac{f}{4R_{in}}v_{rel,f}|v_{rel,f}|-2\upsilon\frac{\left(\tilde{c}_f/c_t\right)^2}{\left[1-\left(\tilde{c}_f/c_t\right)^2\right]}\left[\frac{\rho_f}{\rho_t}\frac{A_{in}}{A_t}\frac{f}{4R_{in}}v_{rel,f}|v_{rel,f}|+gsen\theta\right]$$

$$\frac{dv_f}{d_t}-\frac{g}{c_f}\left\{\left(\frac{\tilde{c}_f}{c_f}\right)+2\upsilon^2\,\frac{R_{in}}{e}\frac{\rho_f}{\rho_t}\frac{(c_f\tilde{c}_f)/c_t^2}{\left[1-\left(\tilde{c}_f/c_t\right)^2\right]}\right\}\frac{dH}{dt}+2\upsilon\frac{\left(\tilde{c}_f/c_t\right)^2}{\left[1-\left(\tilde{c}_f/c_t\right)^2\right]}\left(\frac{d\dot{u}_x}{dt}\right)$$
$$-\frac{2\upsilon}{\rho_t\tilde{c}_f}\frac{\left(\tilde{c}_f/c_t\right)^2}{\left[1-\left(\tilde{c}_f/c_t\right)^2\right]}\left(\frac{d\sigma_x}{dt}\right) \tag{65}$$
$$=-\frac{f}{4R_{in}}v_{rel,f}|v_{rel,f}|+2\upsilon\frac{\left(\tilde{c}_f/c_t\right)^2}{\left[1-\left(\tilde{c}_f/c_t\right)^2\right]}\left[\frac{\rho_f}{\rho_t}\frac{A_{in}}{A_t}\frac{f}{4R_{in}}v_{rel,f}|v_{rel,f}|+gsen\theta\right]$$

Pipe:

$$-\upsilon\frac{R_{in}}{e}\frac{\rho_f}{\rho_t}\frac{\left(c_f/c_t\right)^2}{\left[1-\left(c_f/c_t\right)^2\right]}\left(\frac{dv_f}{d_t}\right)-\upsilon\frac{R_{in}}{e}\frac{\rho_f}{\rho_t}\frac{g}{c_t}\left(\frac{\tilde{c}_t}{c_t}\right)\frac{\left(c_f/c_t\right)^2}{\left[1-\left(c_f/c_t\right)^2\right]}\frac{dH}{d_t}$$
$$+\left\{1+2\upsilon^2\frac{R_{in}}{e}\frac{\rho_f}{\rho_t}\frac{\left(c_f/c_t\right)^2}{\left[1-\left(c_f/c_t\right)^2\right]}\right\}\left(\frac{d\dot{u}_x}{dt}\right)-\frac{1}{\rho_t c_t}\left(\frac{\tilde{c}_t}{c_t}\right)\left(\frac{d\sigma_x}{dt}\right) \tag{66}$$
$$=\left\{1+2\upsilon^2\frac{R_{in}}{e}\frac{\rho_f}{\rho_t}\frac{\left(c_f/c_t\right)^2}{\left[1-\left(c_f/c_t\right)^2\right]}\right\}\left[\frac{\rho_f}{\rho_t}\frac{A_{in}}{A_t}\frac{f}{4R_{in}}v_{rel,f}|v_{rel,f}|+gsen\theta\right]$$
$$+\upsilon\frac{R_{in}}{e}\frac{\rho_f}{\rho_t}\frac{\left(c_f/c_t\right)^2}{\left[1-\left(c_f/c_t\right)^2\right]}\frac{f}{4R_{in}}v_{rel,f}|v_{rel,f}|$$

$$-\upsilon\frac{R_{in}}{e}\frac{\rho_f}{\rho_t}\frac{\left(c_f/c_t\right)^2}{\left[1-\left(c_f/c_t\right)^2\right]}\left(\frac{dv_f}{d_t}\right)+\upsilon\frac{R_{in}}{e}\frac{\rho_f}{\rho_t}\frac{g}{c_t}\left(\frac{\tilde{c}_t}{c_t}\right)\frac{\left(c_f/c_t\right)^2}{\left[1-\left(c_f/c_t\right)^2\right]}\frac{dH}{d_t}$$
$$+\left\{1+2\upsilon^2\frac{R_{in}}{e}\frac{\rho_f}{\rho_t}\frac{\left(c_f/c_t\right)^2}{\left[1-\left(c_f/c_t\right)^2\right]}\right\}\left(\frac{d\dot{u}_x}{dt}\right)+\frac{1}{\rho_t c_t}\left(\frac{\tilde{c}_t}{c_t}\right)\left(\frac{d\sigma_x}{dt}\right)$$
$$=\left\{1+2\upsilon^2\frac{R_{in}}{e}\frac{\rho_f}{\rho_t}\frac{\left(c_f/c_t\right)^2}{\left[1-\left(c_f/c_t\right)^2\right]}\right\}\left[\frac{\rho_f}{\rho_t}\frac{A_{in}}{A_t}\frac{f}{4R_{in}}v_{rel,f}\left|v_{rel,f}\right|+gsen\theta\right] \quad (67)$$
$$+\upsilon\frac{R_{in}}{e}\frac{\rho_f}{\rho_t}\frac{\left(c_f/c_t\right)^2}{\left[1-\left(c_f/c_t\right)^2\right]}\frac{f}{4R_{in}}v_{rel,f}\left|v_{rel,f}\right|$$

Real axial wave velocities (68) and (69) include the effects of Poisson coupling (FSI).

$$\tilde{c}_f=\sqrt{0{,}5\left[q^2-\left(\sqrt{q^4-4c_f^2c_t^2}\right)\right]} \quad (68)$$

$$\tilde{c}_t=\sqrt{0{,}5\left[q^2+\left(\sqrt{q^4-4c_f^2c_t^2}\right)\right]} \quad (69)$$

$$q^2=c_f^2+c_t^2+2\upsilon^2\left(\frac{\rho_f}{\rho_t}\right)\left(\frac{R_{in}}{e}\right)c_f^2 \quad (70)$$

A convenient way to represent equations (64) and (65), (66) and (67) respectively is:

$$\alpha_f\left(\frac{dv_f}{d_t}\right)\pm\beta_f\frac{dH}{d_t}+\upsilon\gamma_f\left(\frac{d\dot{u}_x}{dt}\right)\pm\upsilon\delta_f\left(\frac{d\sigma_x}{dt}\right)=q_f\left(\dot{u}_x,v_f\right) \quad (71)$$

$$\upsilon\alpha_t\left(\frac{dv_f}{d_t}\right)\pm\upsilon\beta_t\frac{dH}{d_t}+\gamma_t\left(\frac{d\dot{u}_x}{dt}\right)\pm\delta_t\left(\frac{d\sigma_x}{dt}\right)=q_t\left(\dot{u}_x,v_f\right) \quad (72)$$

Coefficients $\alpha_f,\alpha_t,\beta_f,\beta_t,\gamma_f,\gamma_t,\delta_f,\delta_t$ represent the corresponding coefficients from equations (64) to (67). The functions $q_f\left(\dot{u}_x,v_f\right)$ and $q_t\left(\dot{u}_x,v_f\right)$ represent the right-hand side of equations (64) to (67).

Integrating compatibility equations results in a system of four equations and four unknowns P(x,t), v(x,t), σ(x,t), and $\dot{u}$ (x,t). This 4x4 system will be used to obtain the solution for points inside the grid.

3.5.1 Computational grids

The computational sections used in classical HT theory is the starting point. They are based on characteristic lines along which pressure waves propagate. The grid spacings (*Δx* e *Δt*) are constant (Lavooij & Tijsseling, 1991). Following Tijsseling (1993) work of, the pressure wave grid $\left(\tilde{c}_f = \Delta x/\Delta t\right)$ will be used.

3.5.2 Convergence and stability

For an accurate numerical solution of a partial differential equation (PDE), finite difference approximations must satisfy the conditions of convergence and stability (Smith et al., 1985).

Convergence:

A finite difference formulation is considered convergent if the exact solution of the finite difference equation tends to the exact solution of the PDE as Δx and Δt approach zero (Chaudhry, 2014).

Stability:

Stability of a finite difference scheme can be investigated using a method developed by Von Neumann. In this method, applicable only to linear equations, the errors in the numerical solution at a particular time are expressed as a Fourier series. It is then determined whether these errors decrease or increase with time. A scheme is said to be stable if the errors decay with time and unstable if the errors grow with time. Thus, it can be shown that the finite difference scheme is stable if (Chaudhry, 2014):

$$\Delta x \geq c.\Delta t \tag{73}$$

This condition is known as the Courant-Friedrich-Lewy (CFL) stability condition. The Courant number (CN) is defined as the ratio of the actual wave speed (*c*) to the numerical wave speed (*Δx/Δt*); that is:

$$NC = \frac{c.\Delta t}{\Delta x} \tag{74}$$

Therefore, for the numerical scheme to be stable, the computational time step (*Δt*) and the spatial interval (*Δx*) must be selected such that CN ≤ 1.

3.6 Validation

The code was tested by comparing it with experimental data from the base article (Bergant, Anton et al., 2005) for a simple hydraulic system, in which transients were induced by opening or closing a valve.

Code algorithm for TH with FSI and separation column (SC) can be found in Appendix.

4 RESULTS AND DISCUSSION

In this section, the results of the simulations performed with the developed code will be presented. The inputs for each simulation can be found in Tables 5 and 6, Appendix.

It should be noted that the assignment of certain fluid and material properties, based on available literature data, was necessary since the data was not provided or mentioned in the reference article:

- Specific mass, Young's modulus, roughness, and Poisson's ratio of the material used;
- Experimental temperature;
- Type of valve used and discharge coeficiente.

4.1 Tests

A numerical and experimental analysis of HT is presented for two different cases of initial flow velocity v_0 = {0,30; 1,40} m/s at a constant static head in the reservoir of 22 m.

Numerical results from code are compared with experimental data at midpoint of the pipe and valve. Computational runs were performed for a rapid closure of the valve fixed rigidly at the downstream end of the pipe. The valve closure time is tc = 0.009 s. Simulation inputs are listed in Tables 5 and 6 in Appendix.

4.1.1 Comparison with experimental data for an initial flow velocity of 0.30 m/s

Figure 4 shows results of the simulations for the partitions Nx = {16, 32, 64, 128}, v_0 = 0.30 m/s, and ψ = 1, along with experimental data for the midpoint of pipe. For validation purposes, ψ = 1 was chosen as the weighting factor used by reference researchers in the field.

Traditionally, a smaller number of partitions is used in HT analysis, but a larger number should provide more accurate results (convergence and stability criteria) (Bergant, Anton et al., 2005).

Figura 4. Comparison with experimental data at midpoint of pipe (v_0 = 0,30 m/s e ψ = 1,0).

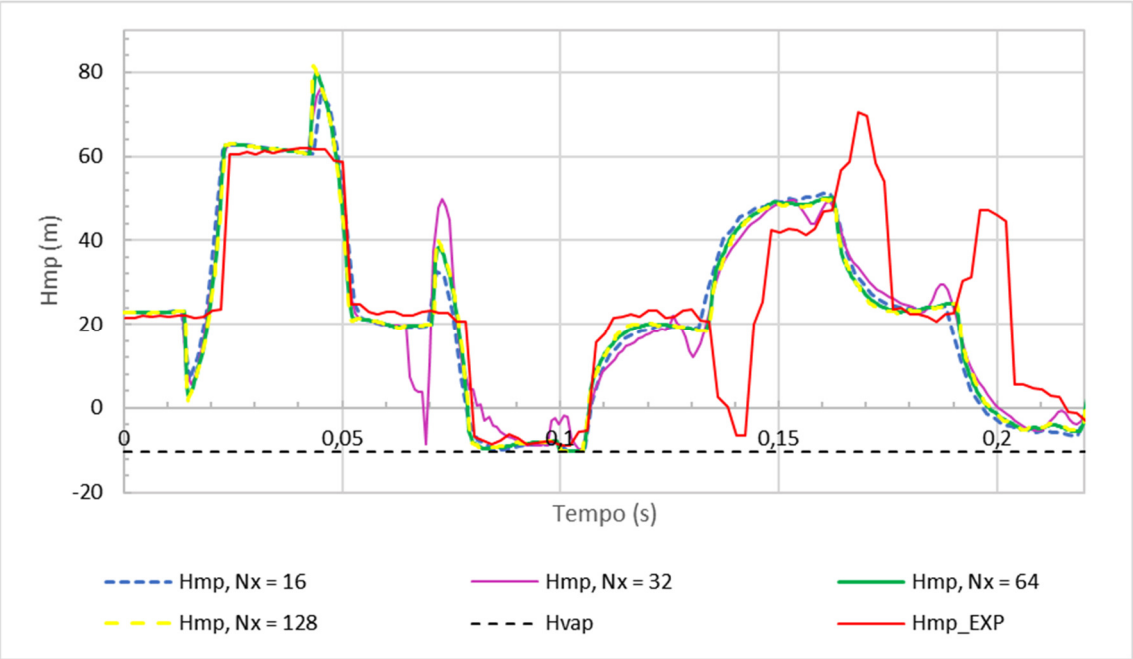

Comparing simulated curves with experimental ones, it can be observed that in the first pressure pulse, curves for *Nx* = {16, 64, 128} successfully captured the increase in head due to the valve closure, as well as the column separation in the interval of 0.08 s to 0.11 s. The pressure peak at 0.04 s in the simulated curves can be explained by the fact that the DVCM model generates unrealistic pressure peaks due to pressure waves reflected in vapor cavities and end limits, as well as the collapse of multicavities (Simpson, Bergant, 1994a).

In Table 1, focusing on the first pressure peak, the maximum head values at the midpoint of pipe and the corresponding times are compiled for the simulations and experiment.

Table 1. Maximum Hmp and occurrence time for each Nx, v_0 = 0,30 m/s e ψ = 1,0.

Nx	$Hmp_{máx}$ (m)	t (s)	Hmp_{max}* (m)[1]	t* (s)[2]

[1] Maximum head of the simulated curves at the midpoint of the pipe, when disregarding the unrealistic pressure peak.

[2] Time at which the maximum head of the simulated curves occurs at the midpoint of the pipe, when disregarding the unrealistic pressure peak.

16	74,92	0,043	62,77	0,026
32	76,20	0,044	62,85	0,025
64	79,88	0,044	62,97	0,025
128	81,47	0,043	63,08	0,025
Experimental	61,84	0,031	61,84	0,031

The objective of this table was to demonstrate that when disregarding the unrealistic pressure peaks resulting from the adopted DVCM model, the maximum captured pressures are very close to the experimentally obtained values, differing at most by 2% (maximum Hmp* difference in $Nx = 128$). Additionally, the occurrence times are approximately identical.

Simulation with $Nx = \{16, 64, 128\}$ is able to predict the second head rise, although in a damped manner. This damping can be explained by use of linear interpolations to solve the PDEs (TIJSSELING, 1993). However, these dampings have the drawback of not capturing real pressure oscillations.

The pressure drop at 0.015 s is due to the globe valve used in the simulated numerical model. It is evident from the comparison that the valve used in the experiment differs from the modeled one.

The curve for $Nx = 32$ generates non-real pressure oscillations throughout the simulation, which can be attributed to pressure waves reflected at the boundaries when adopting the partition 32.

Figure 5 presents the results of the simulations for the partitions $Nx = \{16, 32, 64, 128\}$, $v_0 = 0{,}30$ m/s e $\psi = 1$, along with experimental data at valve.

Figure 5. Comparison with experimental data at valve (v_0 = 0,30 m/s e ψ = 1,0).

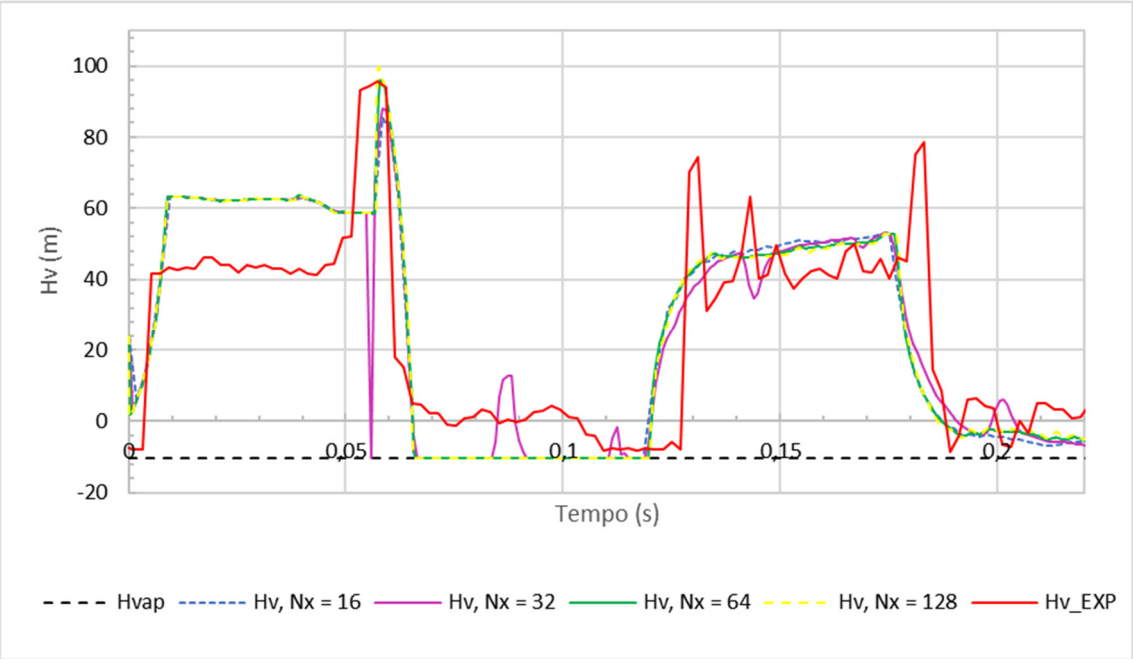

Comparing the simulated curves with the experimental curve, it can be observed that for the first pressure pulse, curves of *Nx* = {16, 32, 64, 128} captured the moment of head elevation. However, only *Nx* = {64} obtained a maximum head value close to experimental data (with a slight upward difference). Apart from the previous observations, the values obtained from the simulation curves do not represent the experimental data, as compiled in Table 2. This discrepancy can be explained by the choice of the valve in the numerical model, which differs from the one used in the experiment.

Table 2. Maximum Hv and occurrence time for each Nx, v_0 = 0,30 m/s e ψ = 1,0.

Nx	Hmáx (m)	t (s)
16	85,57	0,058
32	87,87	0,058
64	96,01	0,058
128	99,69	0,058
Experimental	95,5	0,057

The curve for *Nx* = 32 generates non-real pressure oscillations throughout the simulation, which can be attributed to pressure waves reflected at the boundaries when using a partition of 32.

4.1.2 Comparative analysis with experimental data for an initial flow velocity of 1,40 m/s

Figure 6 displays the results of the simulations for the partitions Nx = {16, 32, 64, 128}, v_0 = 1,40 m/s e ψ = 1, along with experimental data. For the same reasons explained in section 4.1.1, ψ = 1was chosen.

Figura 6. Comparative analysis with experimental data at midpoint of pipeline (v_0 = 1,40 m/s e ψ = 1,0).

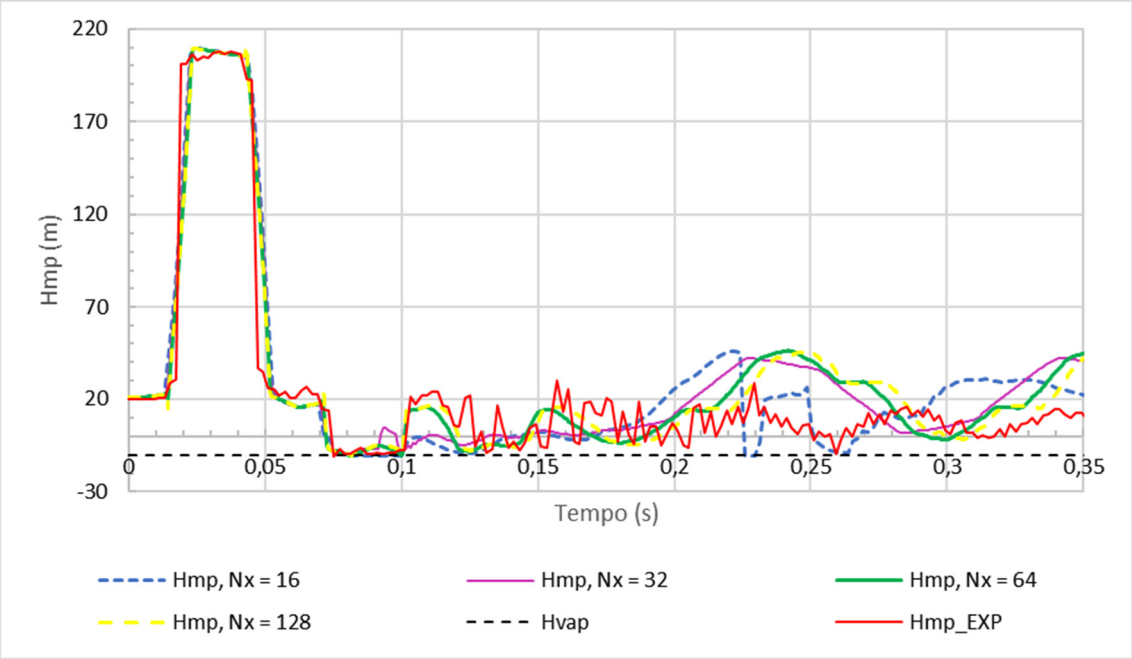

When comparing simulated curves with experimental data, it is observed that in the first pressure pulse, curves for Nx = {16, 32, 64, 128} successfully capture the increase in head due to valve closure, as well as the column separation in the interval 0.07 s - 0.09 s.

For times beyond 0.1 s, the simulations fail to capture the oscillatory behavior observed in the experimental data, which reflects the complexity of the flow due to pressure wave reflections.

Due to the higher initial fluid flow rate, there is no initial pressure drop resulting from the closure of the globe valve used in the simulated numerical model, as shown in Figure 4.

Table 3 compiles maximum head values at midpoint of pipeline and corresponding occurrence times for simulations and experiments.

Tabela 3. Maximum Hmp and occurrence time for each Nx, v_0 = 1,40 m/s e ψ = 1,0.

Nx	Hmáx (m)	t (s)
16	209,10	0,026
32	209,20	0,025
64	209,30	0,024
128	211,50	0,043
Experimental	207,8	0,042

From Table 3, it can be observed that the maximum head values at midpoint of pipeline are slightly higher (0.67% for *Nx* = {16, 32, 64} and 1.78% for *Nx* = {128}) compared to the experimental values. In the cases of *Nx* = {16, 32, 64}, there was an advance in the pressure pulse by approximately 0.17 s, while for *Nx* = {128}, it can be considered that the time of capturing the maximum pressure was the same as experimental value.

The objective of this table was to demonstrate that when disregarding the unrealistic pressure peaks resulting from the adopted DVCM model, the captured maximum pressures are very close to experimental values, differing at most by 2% (Hmp* in *Nx* = 128), and occurrence times are approximately identical.

Figure 7 displays results of simulations for partitions *Nx* = {16, 32, 64, 128}, v_0 = 1,40 m/s e ψ = 1, along with experimental data at valve.

Figure 7. Comparison with experimental data at valve (v_0 = 1,40 m/s e ψ = 1,0).

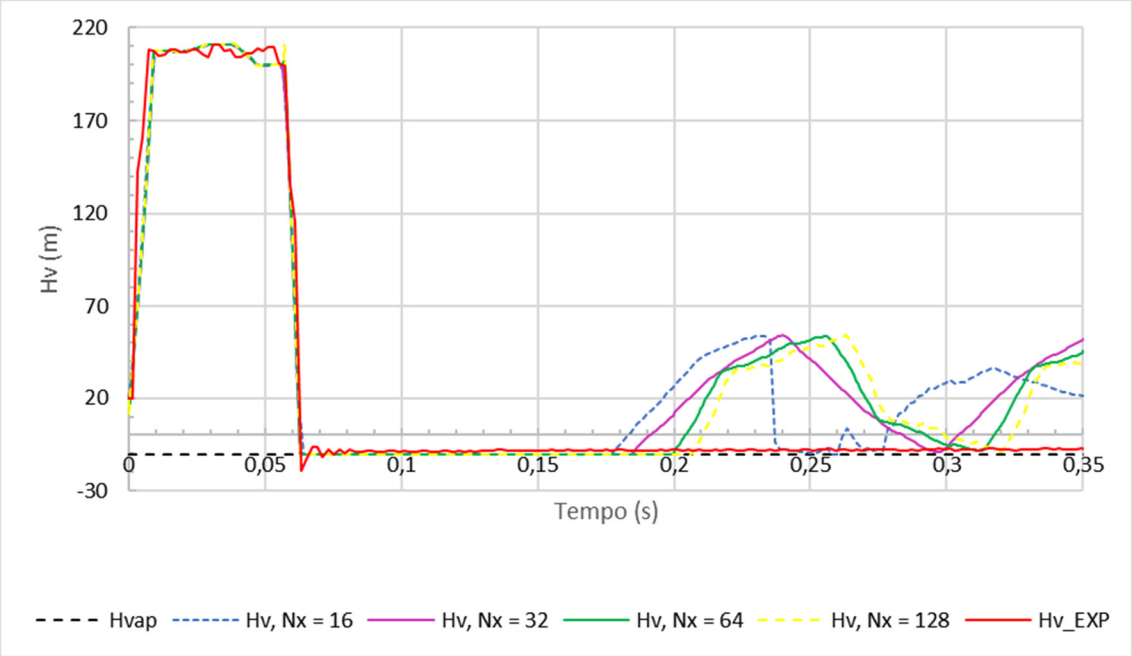

In Table 4, maximum head values at valve and corresponding occurrence times are presented for each *Nx* simulation and experimental data.

Table 4. Maximum Hv and occurrence time for each Nx, v_0 = 1,40 m/s e ψ = 1,0.

Nx	Hmáx (m)	t (s)
16	211,00	0,038
32	211,10	0,037
64	211,10	0,038
128	211,40	0,039
Experimental	210,9	0,038

In comparing simulation results with experimental data, it can be observed that the curves for *Nx* = {16, 32, 64, 128} successfully captured the increase in head due to valve closure, with similar timing and magnitude, as shown in Table 4. They also captured the column separation within the range of 0.06 s to 0.18 s.

For times greater than 0.18 s, simulations exhibit oscillatory behavior that differs from the experimental data. This can be attributed to the fact that in experiment, the valve was axially free, allowing for damping of the pressure pulse at the valve. In contrast, the simulations with a fixed valve are more sensitive to effects of pressure wave reflections.

5 CONCLUSIONS

In this work was presented implementation of Python® code for simulating two-phase flow in a liquid-filled pipe, with without column separation, including combined fluid-structure interaction effects,. Governing equations in one dimension (1D), derived from integration of general three-dimensional (3D) equations for fluid and structure, were used. Fluid structure interaction mechanism included Poisson and friction couplings. Derived equations are valid for phenomena with long wavelength behavior, characteristic of pipes that respond axially and where the fluid wavelength is large compared to the pipe diameter.

For the fluid, Darcy-Weisbach friction model and DVCM model for column separation effects were used as boundary conditions. The basic equations valid for the pipe in question were formulated as a set of four hyperbolic PDEs solved using the method of characteristics, which is considered in the literature to be the best solution for hyperbolic problems where disturbances propagate at constant velocities.

The FSI TH SC model was validated using experimental data from the base article (BERGANT, ANTON et al., 2005) provided by author.

For the available experimental data, proposed model using DVCM with fluid-structure coupling provided a good fit between experimental and numerically simulated data for the first pressure peak at the two evaluated cavitation severity levels (v_0 = 0.30 m/s and v_0 = 1.40 m/s), with slightly better results for the v_0 = 1.40 m/s experiment. This is because the Darcy-Weisbach friction term is capable of predicting the pressure at the first peak, but as the wave propagates, the pressure damping is not sufficient (KWON, 2007).

Theoretical and experimental results were compared. Considering the complexity of the studied phenomenon and the assumptions made for the developed numerical model, combined with the simplicity of DVCM model, maximum manometric head and occurrence time of the first two-phase flow with column separation were accurately predicted.

6 REFERENCES

[1] ALMEIDA, R. S. P. ***Modelo Numérico para Cálculo do Transitório Hidráulico e Interação Fluido-Estrutura em Sistemas de Transporte de Fluidos***. 2018. 108 p. Dissertação (Mestrado em Tecnologia Nuclear) – Instituto de Pesquisas Energéticas e Nucleares - IPEN, São Paulo, 2018.

[2] BERGANT, A. ***Kavitacijski tok med prehodnimi rezimi v cevnih sistemih. (Transient cavitating flow in pipelines.)***. 1992. PhD Thesis – University of Ljubljana, Ljubljana, Slovenia, 1992.

[3] BERGANT, A. et al. Water hammer with column separation: A review of research in the twentieth century. Citation Key: Simpson, Angus & Tijsseling, Rris. (2004). Water hammer with column separation: a review of research in the twentieth century. Anxiety Stress and Coping - ANXIETY STRESS COPING., 2004. Disponível em: https://www.researchgate.net/publication/228851496_Water_hammer_with_column_separation_a_review_of_research_in_the_twentieth_century. Acesso em: 07 dez. 2021.

[4] BERGANT, A.; SIMPSON, A. R.; TIJSSELING, A. S. Water hammer with column separation: A historical review. ***Journal of Fluids and Structures***, v. 22, n. 2, p. 135–171, fev. 2006. Disponível em: https://linkinghub.elsevier.com/retrieve/pii/S0889974605001520. Acesso em: 06 dez. 2022.

[5] BERGANT, Anton; KARAD IÆ, U.; VÍTKOVSKÝ, J.; VU ANOVIÆ, I.; SIMPSON, A. A discrete gas-cavity model that considers the frictional effects of unsteady pipe flow. ***Stronjniski Vestnik-Journal of Mechanical Engineering***, v. 5111, p. 692–710, jan. 2005.

[6] BERGANT, Anton; SIMPSON, A. R. Pipeline Column Separation Flow Regimes. ***Journal of Hydraulic Engineering***, v. 125, n. 8, p. 835–848, ago. 1999. Disponível em: https://ascelibrary.org/doi/10.1061/%28ASCE%290733-9429%281999%29125%3A8%28835%29. Acesso em: 06 dez. 2022.

[7] BERGANT, Anton; SIMPSON, A. R.; TIJSSELING, A. S. Water hammer with column separation: A historical review. ***Journal of Fluids and Structures***, v. 22, n. 2, p. 135–171, 2006.

[8] BERGANT, Anton; TIJSSELING, A. S.; VÍTKOVSKÝ, J. P.; COVAS, D. I. C.; SIMPSON, A. R.; LAMBERT, M. F. Parameters affecting water-hammer wave attenuation, shape and timing - Part 1: Mathematical tools. ***Journal of Hydraulic Research***, v. 46, n. 3, p. 373–381, 2008.

[9] BERNARD, D. ***NUMERIC MODELLING OF WATER HAMMER EFFECTS IN PENSTOCKS***. 2013. Master – University of Ottawa, Department of Civil Engineering, Ottawa, Canada, 2013.

[10] CHAUDHRY, M. H. ***Applied Hydraulic Transients***. New York, NY: Springer New York, 2014. Disponível em: http://link.springer.com/10.1007/978-1-4614-8538-4. Acesso em: 06 dez. 2022.

[11] CHAUDHRY, M. H.; HOLLOWAY, M. B. Stability of method of characteristics. In: WATER FOR RESOURCE DEVELOPMENT, 1984, p. 216–220.

[12] CROWE, C. T.; ELGER, D. F.; WILLIAMS, B. C.; ROBERSON, J. A. ***Engineering fluid mechanics***. 9th ed, Hoboken, NJ: Wiley, 2009. 1 p.

[13] FAN, D.; TIJSSELING, A. Fluid-Structure Interaction With Cavitation in Transient Pipe Flows. ***Journal of Fluids Engineering***, v. 114, n. 2, p. 268–274, 1 jun. 1992. Disponível em: https://asmedigitalcollection.asme.org/fluidsengineering/article/114/2/268/410883/FluidStructure-Interaction-With-Cavitation-in. Acesso em: 11 dez. 2022.

[14] FANELLI, M. ***Hydraulic Transients with water column separation, IAHR Working Group 1971-1991, Synthesis Report, Delft:IAHR and Milan:ENELCRIS***. [S.l: s.n.], 2000.

[15] HALLIWELL, A. R. Velocity of a Water-Hammer Wave in an Elastic Pipe. ***Journal of the Hydraulics Division***, v. 89, n. 4, p. 1–21, jul. 1963. Disponível em: https://ascelibrary.org/doi/10.1061/JYCEAJ.0000897. Acesso em: 07 dez. 2022.

[16] HARRIS, C. R.; MILLMAN, K. J.; VAN DER WALT, S. J.; GOMMERS, R.; VIRTANEN, P.; COURNAPEAU, D.; WIESER, E.; TAYLOR, J.; BERG, S.; SMITH, N. J.; KERN, R.; PICUS, M.; HOYER, S.; VAN KERKWIJK, M. H.; BRETT, M.; HALDANE, A.; DEL RÍO, J. F.; WIEBE, M.; PETERSON, P.; GÉRARD-MARCHANT, P.; SHEPPARD, K.; REDDY, T.; WECKESSER, W.; ABBASI, H.; GOHLKE, C.; OLIPHANT, T. E. Array programming with NumPy. ***Nature***, v. 585, n.

7825, p. 357–362, 17 set. 2020. Disponível em: https://www.nature.com/articles/s41586-020-2649-2. Acesso em: 20 mar. 2023.

[17] HOLLOWAY, M. B.; HANIF CHAUDHRY, M. Stability and accuracy of waterhammer analysis. ***Advances in Water Resources***, v. 8, n. 3, p. 121–128, set. 1985. Disponível em: https://linkinghub.elsevier.com/retrieve/pii/0309170885900521. Acesso em: 02 maio 2023.

[18] IAHR. ***Hydraulic transients with water column separation: IAHR Working Group 1971 - 1991 synthesis report***. Delft: International Association of Hydraulic Engineering and Research, 2000. 782 p.

[19] JENSEN, R.; LARSEN, J.; LASSEN, K.; MANDØ, M.; ANDREASEN, A. Implementation and Validation of a Free Open Source 1D Water Hammer Code. ***Fluids***, v. 3, n. 3, p. 64, 3 set. 2018. Disponível em: http://www.mdpi.com/2311-5521/3/3/64. Acesso em: 06 dez. 2022.

[20] KORTEWEG, D. J. Ueber die Fortpflanzungsgeschwindigkeit des Schalles in elastischen Röhren. ***Annalen der Physik und Chemie***, v. 241, n. 12, p. 525–542, 1878. Disponível em: https://onlinelibrary.wiley.com/doi/10.1002/andp.18782411206. Acesso em: 07 dez. 2022.

[21] LAVOOIJ, C. S. W.; TIJSSELING, A. S. Fluid-structure interaction in liquid-filled piping systems. ***Journal of Fluids and Structures***, v. 5, n. 5, p. 573–595, set.

1991. Disponível em: https://linkinghub.elsevier.com/retrieve/pii/S0889974605800064. Acesso em: 19 dez. 2022.

[22] LESLIE, D. J.; VARDY, A. E. Practical Guidelines for fluid-structure interaction in pipelines: A review. 2001.

[23] MOODY, F. J. ***Introduction to unsteady thermofluid mechanics***. New York: Wiley, 1990. 654 p.

[24] ROCHA, M. S. ***Influência do fator de atrito no cálculo do transiente hidráulico***. 1998. Mestrado – Universidade Estadual de Campinas, Campinas, 1998.

[25] ROCHA, R. G. ***Interação Fluido-Estrutura em sistemas de tubulações conduzindo líquidos via Método de Glimm***. 2011. Doutorado – Universidade Federal Fluminense, Rio de Janeiro, 2011.

[26] SHAMLOO, H.; NOROOZ, R.; MOUSAVIFARD, M. Investigation of Parameters Affecting Discrete Vapour Cavity Model. ***International Journal of Civil Engineering and Geo-Environment***, v. 5, , jan. 2014. Disponível em: http://ijceg.ump.edu.my

[27] SHARP, B. B.; SHARP, D. B. ***Water hammer: practical solutions***. London : New York: Arnold ; Halsted Press, 1996. 172 p.

[28] SIMPSON, A. R.; BERGANT, A. ***Angus Ross; Bergant, Anton Numerical comparison of pipe-column-separation models***. Journal of Hydraulic Engineering[S.l: s.n.], 1994. a. Disponível em: http://www.asce.org/Content.aspx?id=29734

[29] SIMPSON, A. R.; BERGANT, A. Numerical Comparison of Pipe-Column-Separation Models. ***Journal of Hydraulic Engineering***, v. 120, n. 3, p. 361–377, mar. 1994. b. Disponível em: https://ascelibrary.org/doi/10.1061/%28ASCE%290733-9429%281994%29120%3A3%28361%29. Acesso em: 08 dez. 2022.

[30] SIMPSON, A.; WYLIE, E. Towards an improved understanding of water hammer column separation in pipelines. The Institution of Engineers, Australia, p. 113–120, 1989. 31. ed., Disponível em: http://trove.nla.gov.au/version/33864621

[31] SMITH, G. D.; SMITH, G. D.; SMITH, G. D. S. ***Numerical solution of partial differential equations: finite difference methods***. [S.l.]: Oxford university press, 1985.

[32] TIJSSELING, A. S. Fluid-structure interaction in liquid-filled pipe systems: A review. ***Journal of Fluids and Structures***, v. 10, n. 2, p. 109–146, 1996.

[33] TIJSSELING, A. S.; LAVOOIJ, C. S. W. Fluid-structure interaction in compliant piping systems. 1989, Cambridge, UK. p. 85–100.

[34] TIJSSELING, A. S.; LAVOOIJ, C. S. W. ***Water hammer with fluid-structure interaction***. Applied Scientific Research[S.l.]: Kluwer Academic Publishers, 1990.

[35] TIJSSELING, A. S., Tijsseling. ***Fluid-structure interaction in case of waterhammer with cavitation.*** 1993. Delft University of Technology, Delft , Netherlands, 1993.

[36] TULLIS, J. P. ***Hydraulics of pipelines: pumps, valves, cavitation, transients***. New York: Wiley, 1989. 266 p.

[37] U.S. NUCLEAR REGULATORY RESEARCH. ***Screening Reactor Steam/Water Piping Systems for Water Hammer***. NUREG-CR-6519[S.l: s.n.], 1997.

[38] VIRTANEN, P. SciPy 1.0: fundamental algorithms for scientific computing in Python. ***Nature Methods***, v. 17, n. 3, p. 261–272, 2 mar. 2020. Disponível em: http://www.nature.com/articles/s41592-019-0686-2. Acesso em: 20 mar. 2023.

[39] WIGGERT, D. C.; TIJSSELING, A. S. Fluid transients and fluid-structure interaction in flexible liquid-filled piping. ***Applied Mechanics Reviews***, v. 54, n. 5, p. 455–481, 1 set. 2001. Disponível em: https://asmedigitalcollection.asme.org/appliedmechanicsreviews/article/54/5/455/445230/Fluid-transients-and-fluidstructure-interaction-in

[40] WYLIE, E. B.; STREETER, V. ***Fluid Transients***. [S.l.]: McGraw-Hill Inc., 1978.

[41] WYLIE, E. Benjamin; STREETER, V. L.; SUO, L. ***Fluid transients in systems***. Englewood Cliffs, NJ: Prentice Hall, 1993. 463 p.

APPENDIX

HYDRAULIC TRANSIENT WITH FLUID STRUCTURE INTERACTION AND COLUMN SEPARATION

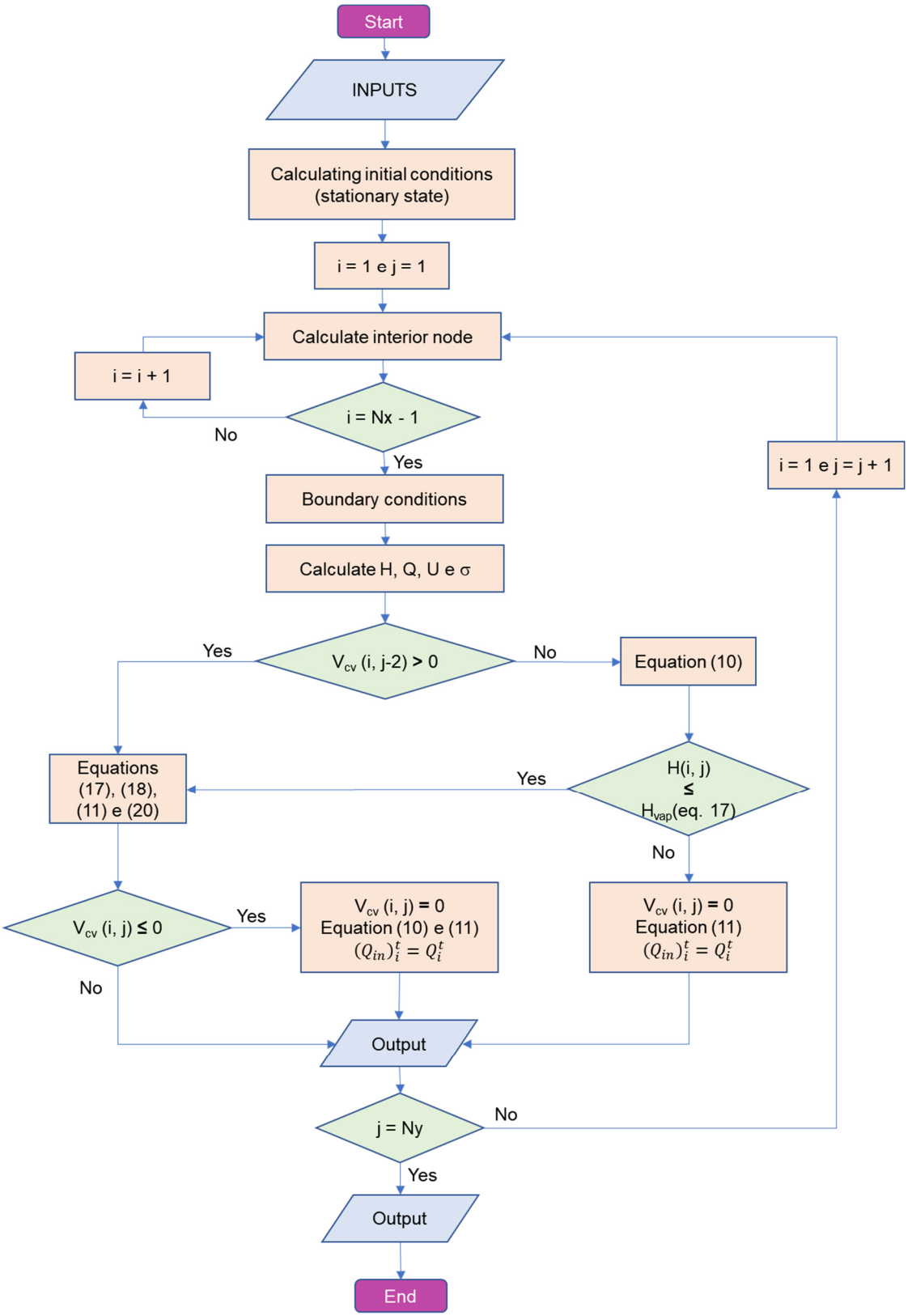

First it is necessary to calculate the unknowns H, v, σ_x and $\dot{u}_x$, then block with $V_{cv}(i, j-2) > 0$ investigates the presence of vapor cavity in the previous time step. If cavity exists, it is assumed that the current time interval should be treated as a pressure threshold. If the node is calculated as a pressure threshold, the calculations are followed by a check to see if the vapor cavity is less than or equal to zero. If this is true, it is assumed that the vapor cavity has collapsed, but the pressure has not risen above the vaporization pressure of the fluid and consequently there is a new check of the calculated head and the vaporization head ($H_i^j \leq H_{vap}$). This loop is reapeted for all *j*.

Table 5. Properties and parameters for the simulation v_0 = 0,30 m/s e ψ = 1,0.

Properties and parameters		
g	9,81	[m/s²]
Pipe		
L	37,23	[m]
Din	2,21E-02	[m]
Rin	1,11E-02	[m]
e	1,63E-03	[m]
E	1,24E+11	[Pa]
roughness	7,00E-06	[m]
rho_t	8940	[kg/m³]
coef. Poisson	0,34	[dimensionless]
theta	0,0545	[rad]
tc	9,00E-03	[s]
Pext	1,00E+05	[Pa]
Fluid		
rho_f	998,2	[kg/m³]
kf	2,10E+09	[Pa]
mi_f	1,00E-03	[kg/m.s]
Hvap	-10,221	[m]
psi	1	[dimensionless]
Initial conditions of system		
Hres	22	[m]
v_0	0,30	[m/s]
U_0	0	[m/s]

Table 6. Properties and parameters for the simulation v0 = 1,40 m/s e ψ = 1,0.

Properties and parameters		
g	9,81	[m/s²]
Pipe		
L	37,23	[m]
Din	2,21E-02	[m]
Rin	1,11E-02	[m]
e	1,63E-03	[m]
E	1,24E+11	[Pa]
roughness	7,00E-06	[m]
rho_t	8940	[kg/m³]
coef. Poisson	0,34	[dimensionless]
theta	0,0545	[rad]
tc	9,00E-03	[s]
Pext	1,00E+05	[Pa]
Fluid		
rho_f	998,2	[kg/m³]
kf	2,10E+09	[Pa]
mi_f	1,00E-03	[kg/m.s]
Hvap	-10,221	[m]
psi	1	[dimensionless]
Initial conditions of system		
H_{res}	22	[m]
v_0	1,40	[m/s]
U_0	0	[m/s]